PNAS RESEARCH ARTICLE | CELL BIOLOGY

Development and characterization of human fetal female reproductive tract organoids to understand Müllerian duct anomalies

Varshini D. Venkata[a,b], M. Fairuz B. Jamaluddin[a,b], Jyoti Goad[a,b], Hannah R. Drury[a,b], Melissa A. Tadros[a,b], Rebecca Lim[a,b], Ajay Karakoti[b,c], Rachel O'Sullivan[d], Yvette Ius[d], Kenneth Jaaback[d], Pravin Nahar[e], and Pradeep S. Tanwar[a,b,1]

Edited by Thomas Spencer, University of Missouri, Columbia, MO; received October 27, 2021; accepted March 30, 2022

Müllerian ducts are paired tubular structures that give rise to most of the female reproductive organs. Any abnormalities in the development and differentiation of these ducts lead to anatomical defects in the female reproductive tract organs categorized as Müllerian duct anomalies. Due to the limited access to fetal tissues, little is understood of human reproductive tract development and the associated anomalies. Although organoids represent a powerful model to decipher human development and disease, such organoids from fetal reproductive organs are not available. Here, we developed organoids from human fetal fallopian tubes and uteri and compared them with their adult counterparts. Our results demonstrate that human fetal reproductive tract epithelia do not express some of the typical markers of adult reproductive tract epithelia. Furthermore, fetal organoids are grossly, histologically, and proteomically different from adult organoids. While external supplementation of WNT ligands or activators in culture medium is an absolute requirement for the adult reproductive tract organoids, fetal organoids are able to grow in WNT-deficient conditions. We also developed decellularized tissue scaffolds from adult human fallopian tubes and uteri. Transplantation of fetal organoids onto these scaffolds led to the regeneration of the adult fallopian tube and uterine epithelia. Importantly, suppression of Wnt signaling, which is altered in patients with Müllerian duct anomalies, inhibits the regenerative ability of human fetal organoids and causes severe anatomical defects in the mouse reproductive tract. Thus, our fetal organoids represent an important platform to study the underlying basis of human female reproductive tract development and diseases.

endometrium | organoid | fallopian tube | Müllerian duct | uterus

Significance

One of the fascinating events in human development is the transformation of Müllerian ducts, a set of simple and uniform tubes, into spatially restricted and highly complex reproductive tract organs and their distinct epithelia. This occurs in a relatively short window of time during fetal development, and any aberrations result in females born with missing or defective organs. How fetal reproductive organs are different from their adult organ counterparts is not well-understood. We developed human fetal fallopian tube and uterine organoids and described differences with adult organ organoids. Fetal organoids can maintain long-term in culture and regenerate epithelium upon transplantation on scaffolds developed from adult organs. Fetal organoids represent a unique platform to study human development and associated disorders.

Müllerian duct anomalies (MDAs) represent a group of developmental disorders related to abnormalities in female reproductive tract organs (1). The incidence rate of MDAs in the general population and fertile women is around 5% (2, 3). Women with fertility problems and recurrent miscarriages have a much higher prevalence of 6 to 15% (2, 3). Müllerian ducts (MDs; also known as paramesonephric ducts) are the paired tubular structures that undergo a highly orchestrated and complex process of differentiation to give rise to the fallopian tubes (FTs), uterus, cervix, and upper vagina (4, 5). In MDA patients, one or more MD-derived organs are either underdeveloped or missing completely (1, 6). Such patients are usually of a normal karyotype 46, XX genetic females and often have functioning ovaries and age-appropriate external genitalia (1). Therefore, these females are generally presented in the clinic in the postpubertal stages with a wide range of gynecological and obstetrical disorders, including infertility and recurrent first-semester miscarriages (3). The clinical presentation of patients is related to the severity of the anatomical defects in MD-derived organs, which range from agenesis of the uterus and vagina to minor uterine cavity malformations (1).

Mayer–Rokitansky–Küster–Hauser (MRKH) syndrome is one the most recognized congenital forms of MDAs, and it affects ∼1 in 4,500 female births. MRKH is further divided into two types. In type I MRKH syndrome, defects are limited to the MD-derived organs, whereas in type II, other organs, such as renal and musculoskeletal systems, are also involved (6). Genome sequencing of MRKH patients has revealed alterations in several key members (*WNT4*, *WNT9B*, *RSPO4*, *LRP10*, *TCF2*) of the WNT pathway (7–9). Studies using mouse models have provided experimental evidence supporting the role of this signaling pathway in MD development and differentiation (5, 10). In mice, the *Wnt4* gene is required for the initiation, invagination, and differentiation of MDs, as shown by the lack of MD development in *Wnt4* knockout mice (11). Wnt9b is required for the caudal extension of MDs, and its loss in mice leads to the absence of the uterus and upper vagina (12). Genetic alterations in

Author contributions: P.S.T. designed research; V.D.V., M.F.B.J., J.G., and P.S.T. performed research; H.R.D., M.A.T., R.L., A.K., R.O., Y.I., K.J., P.N., and P.S.T. contributed new reagents/analytic tools; V.D.V., M.F.B.J., and P.S.T. analyzed data; and V.D.V. and P.S.T. wrote the paper.

The authors declare no competing interest.

This article is a PNAS Direct Submission.

[1]To whom correspondence may be addressed. Email: pradeep.tanwar@newcastle.edu.au.

This article contains supporting information online at http://www.pnas.org/lookup/suppl/doi:10.1073/pnas.2118054119/-/DCSupplemental.

Published July 18, 2022.

β-catenin (*Ctnnb1*), a key mediator of the canonical Wnt signaling, inhibit MD regression in male mice and cause abnormal differentiation of MDs in female mice (10, 13–15). Collectively, these studies in mouse models have highlighted the significance of Wnt signaling in MD development and provided possible clues into the pathogenesis of MRKH syndrome. However, the key differences in human and mouse MD development limit the translation of these studies to patients. For example, uterine gland development occurs postnatally in animal models, including rodents and ungulates (16). In comparison, this process starts during fetal stages in humans and, by 18 wk of gestation, endometrial glands have already formed in the fetal uterus (17, 18). Therefore, human models are required to better understand the pathogenesis of MDAs and guide the development of personalized treatments for these patients.

Organoid technology has provided an unprecedented window into various human developmental processes and allowed us to replicate the organ physiology and the pathological changes that occur during different stages of human diseases (19). More importantly, organoids from even a tiny biopsy can generate enough cellular material required for regenerative treatments, which is especially important for congenital disorders, such as MDAs, where a part or the whole organ system is missing (20). Furthermore, organoids from definitive endoderm have provided insights into the processes underlying the development of human gastrointestinal tract (GIT) organs. It has facilitated our understanding of the complex signaling circuitry that creates organ boundaries, ensures the spatial restriction of different GIT organs, and defines their identities despite their common developmental origin (21). We expect that similar models from MDs will be instrumental in understanding how a simple tube differentiates in a segmental fashion to precisely give rise to spatially restricted and highly complex female reproductive organs. Various groups have now established and characterized organoids from adult female reproductive organs (22). Organoids generated from adult FTs, endometrium, cervix, and vagina have already proven invaluable models to understand the basis of several gynecological diseases (22). Unfortunately, fetal organoid models developed from fetal reproductive tract organs have not been reported to date. Here, we developed human fetal female reproductive organoids that represent a unique platform to investigate human female reproductive development and diseases and provide important insights into the underlying mechanisms. We showed that fetal organoids maintain many of their in vivo features and are significantly different from their adult counterparts. Additionally, we provide evidence that the transplantation of fetal and adult organoids contributes to the regeneration of adult tissues.

Results

Comparative Analysis of Human Fetal and Adult Female Reproductive Tract Epithelium. To understand the fundamental differences between human fetal and adult reproductive tract organs, we collected fetal female reproductive tissue samples ($n = 12$; 9 to 14 wk of gestation; *SI Appendix*, Table S1) and adult premenopausal FTs and uteri ($n = 5$ each) and performed a comparative histopathological analysis (Fig. 1). In humans, MDs first appear around 6 wk of gestation and, by 9 wk, the two MDs fuse to form primitive FTs and a uterus (17, 18). Our gross examination of the fetal tissue specimens at around 10 wk of age showed that FTs and the uterine body are quite distinguishable at this stage of development (Fig. 1*A*). By 13 wk, the fetal reproductive tract has acquired the typical shape

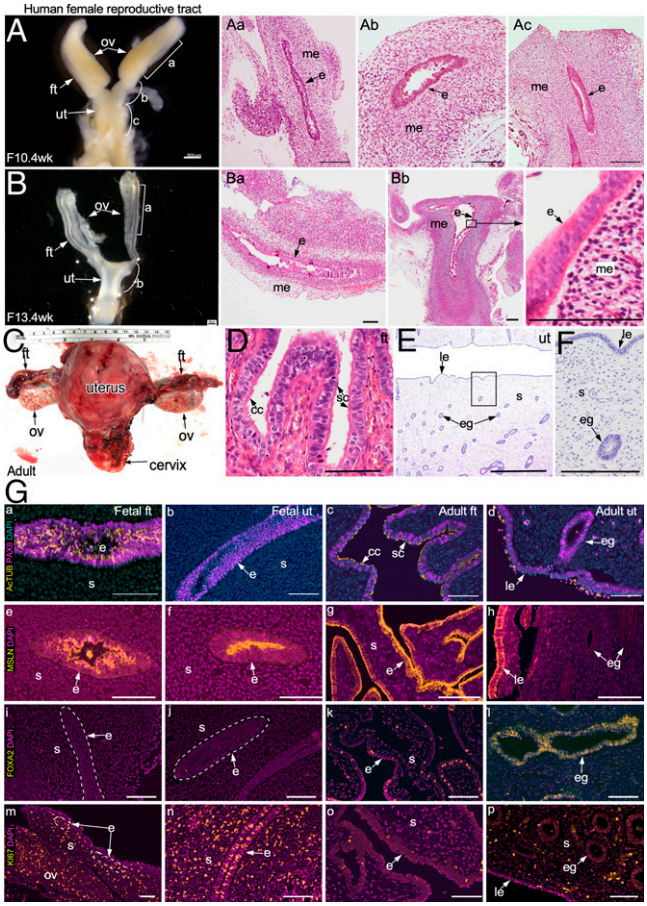

Fig. 1. Gross and histological analysis of human fetal and adult FTs and uterus. (*A*) Gross (*A*) and histological (*A*, *a*–*c*) images of human fetal female reproductive tract at 10.4 wk of gestation ($n = 2$) showing hematoxylin and eosin (H&E)–stained fetal FTs (*A*, *a* and *b*) and uterus (*A*, *c*). (*B*) Gross morphology (*B*) and histology (*B*, *a* and *b*) of human fetal reproductive tract at 13.4 wk of gestation ($n = 3$) showing H&E-stained sections of the FTs (*B*, *a*) and uterus (*B*, *b*). A higher-magnification image of *B*, *b*, *Inset* shows pseudostratified columnar epithelium. (*C*) A representative image of an adult premenopausal female reproductive tract ($n = 3$). (*D*) The adult FT is lined by simple columnar epithelium containing ciliated and secretory cells. (*E* and *F*) Typical histological presentation of the adult uterine epithelium with luminal and glandular epithelial compartments. (*G*) Coimmunostaining for PAX8 (a marker of the MD epithelium) and AcTUB (a ciliated cell marker) in human fetal FTs (*G*, *a*) and uterus (*G*, *b*) and in adult FTs (*G*, *c*) and uterus (*G*, *d*). Immunostaining for mesothelin (MSLN, a marker of coelomic epithelium; *e*–*h*), FOXA2 (a marker of uterine glands; *i*–*l*), and KI67 (a proliferating cell marker; *m*–*p*) in human fetal (*G*, *e*, *f*, *i*, *j*, *m*, and *n*) and adult (*G*, *g*, *h*, *k*, *l*, *o*, and *p*) FTs (*G*, *e*, *g*, *i*, *k*, *m*, and *o*) and uterus (*G*, *f*, *h*, *j*, *l*, *n*, and *p*) ($n = 3$ biological replicates × 12 images per replicate). White dotted lines in *G*, *i*, *j*, and *m* demarcate epithelium from the underlying mesenchyme. cc, ciliated cells; e, epithelium; eg, glandular epithelium; ft, fallopian tubes; le, luminal epithelium; me, mesenchyme; ov, ovary; s, stroma; sc, secretory cells; ut, uterus. (Scale bars, 100 μm unless indicated otherwise.)

of the adult reproductive tract, and both the FTs and the uterus present a clearly defined lumen (Fig. 1 *B* and *C*). Histologically, fetal FTs as well as uteri are lined with pseudostratified columnar epithelium with ovoid or round nuclei that are arranged at basal, intermediate, and superficial levels (Fig. 1 *A*, *a*–*c* and *B*, *a* and *b*). In comparison, adult FTs and uteri are lined with simple columnar epithelium that consists of secretory and ciliated cell types (Fig. 1*D*). Adult uterine epithelium, however, is further subdivided into two compartments, luminal and glandular epithelium (Fig. 1 *E* and *F*). Comparison of the biomarker profile of the epithelial cell types also revealed differences between fetal and adult tissues (*SI Appendix*, Table S2). In adults, both FT and uterine epithelia are composed of cell types expressing PAX8 (secretory type) and Human AcTUB (acetylated tubulin; ciliated type). On

the other hand, only fetal FT epithelium consists of these two cell types, while the fetal uterine epithelium is composed of only PAX8+ secretory cells (Fig. 1 *G*, *a–d* and *SI Appendix*, Fig. S1). Furthermore, cilia in the fetal FT epithelium appear immature and have only one or two ciliary strands (Fig. 1 *G*, *a* and *SI Appendix*, Fig. S1). In comparison, ciliogenesis in mice occurs postnatally, and ciliated cells first appear in the FTs (also known as oviducts) at 3 d of age (23). Mesothelin, a marker of the coelomic epithelium (24), was present exclusively on the apical surface of both the fetal FT and uterine epithelium, whereas its expression was observed across the whole epithelium of the adult FT as well as the luminal but not the glandular epithelium of the adult uterus (Fig. 1 *G*, *e–h*). FOXA2, a known marker of endometrial glands (25), was detected in the uterine glandular epithelium and the mature secretory cells of the adult FT epithelium (Fig. 1 *G*, *i–l* and *SI Appendix*, Table S2). However, its expression was absent in both the fetal FT as well as the uterine epithelia (Fig. 1 *G*, *i* and *j*). This suggests the immature and relatively undifferentiated nature of both the fetal FT and the uterine epithelial cells. Accordingly, both fetal FT and uterine epithelial as well as mesenchymal cells were more proliferative (KI67+) than their adult counterparts (Fig. 1 *G*, *m–p*), suggesting that fetal epithelia mostly consist of immature epithelial progenitors. Collectively, these results highlight some of the key differences between the fetal and adult epithelia of human FTs and uteri.

Propagation of Mouse MD-Derived Organoids. Due to the physical nature of the elective termination procedure, we were often unable to retrieve the reproductive tract tissues from the macerated products of conception. Therefore, we decided to use mouse fetal tissues to standardize our organoid culture and propagation protocols before applying them to human fetal samples. Active WNT signaling is a critical requirement for the growth and maintenance of adult reproductive tract tissue-derived organoids (22). Hence, we first examined if this signaling pathway is active during MD development and differentiation using TCF-GFP mice, a well-established Wnt reporter mouse model (26). In these mice, nuclear green fluorescent protein (GFP) expression is exclusively limited to cells with active Wnt signaling (27). Examination of TCF-GFP fetal tissues at 13.5 and 14.5 d postcoitus (embryonic day 13.5 [E13.5] and E14.5) showed high TCF-GFP expression in MDs, albeit at a lower level than the Wolffian ducts (WDs), suggesting that Wnt signaling is active during the early stages of MD development (Fig. 2 *A*, *a–d*). At E16.5, when MDs start to differentiate, TCF-GFP expression was more intense in the upper segment that ultimately forms FTs than in the lower segment that gives rise to the uterus (Fig. 2 *A*, *e–g*). Quantification using fluorescence-activated cell sorting (FACS) of EpCAM+ GFP+ cells from E16.5 MDs of TCF-GFP mice confirmed a higher percentage of GFP+ cells in the epithelium of presumptive FT compared with the uterus (Fig. 2 *A*, *h*). By E18.5 and postnatal day 1 (P1), mouse FTs had already acquired a spiral shape, and the TCF-GFP expression was much higher in the FTs than in the uterus (Fig. 2 *A*, *i–n*). Our analysis of the two bona fide downstream targets of canonical WNT signaling, TCF1 and LEF1, in human fetal reproductive tracts revealed a differential expression pattern that suggested a higher Wnt signaling activity in the FTs relative to uteri, a trend similar to that in the mouse reproductive tract (*SI Appendix*, Fig. S2). This highlights the dynamic regional differences in the Wnt activity in the MDs, suggesting the context-dependent role of Wnt signaling in the development of female reproductive tracts. Next, to confirm if MDs and the neonatal reproductive tract also express the major regulators of Wnt signaling, we analyzed the expression of Wnt ligands (Wnt7 and Wnt4) and the downstream targets (Lgr5 and Axin2) using in situ hybridization in tissue samples representing E14.5 MD, E16.5 MD, and P1 neonatal reproductive tract (Fig. 2*B*). *Wnt7a* expression was mainly limited to epithelial cells at all these stages of development (Fig. 2 *B*, *a–d*). *Wnt4* was strongly expressed by stromal cells, but a weak expression was also observed in the epithelial cells of the MDs (E14.5, E16.5) and the FTs and uterus at P1 (Fig. 2 *B*, *e–h*). *Lgr5* and *Axin2* were expressed in a punctate manner by a minor population of the epithelial cells (Fig. 2 *B*, *i–p*). *Axin2* also marked mesenchymal/stromal cells, whereas *Lgr5* was expressed in very few stromal cells (Fig. 2 *B*, *i–p*).

Given our Wnt signaling analysis, we reasoned that MDs acquire FT fate under high Wnt conditions and uterine fate in a low Wnt environment. Therefore, in order to direct E14.5 MD epithelial cells to either the FT or uterine fate, we formulated three different culture media representing high Wnt conditions (25% Wnt3a-R-Spondin-Noggin conditioned medium, WRN CM; epidermal growth factor, EGF; fibroblast growth factor 10, FGF10; WRNEF) and low Wnt conditions (25% R-spondin CM, Noggin, EGF, FGF10, ±CHIR99201; RNEFC or RNEF) (*SI Appendix*, Table S3). MD epithelium was dissected from the underlying mesenchyme, and the epithelial fragments were enzymatically digested to obtain a single-cell suspension. Twenty thousand cells were plated per 50 µL basement membrane extract (BME) droplet and subsequently cultured in the above three culture media (Fig. 2*C*). Under high Wnt conditions (WRNEF), organoids grew from single cells and reached >1 mm in size within 2 wk of culture (Fig. 2*C*). While organoids also developed in the low Wnt conditions (RNEFC), they were relatively smaller in size than those cultured under high Wnt conditions (Fig. 2*C*). On the other hand, cells plated in RNEF culture medium did not develop healthy organoids (Fig. 2*C*), indicating that the addition of CHIR99201, a glycogen synthase kinase inhibitor (28), was essential for the growth of these organoids. To determine if modulation of Wnt signaling is sufficient to redirect the fate of committed FT and uterine epithelial cells, we isolated epithelial cells from E16.5 MDs and cultured them in high (WRNEF medium; *SI Appendix*, Table S3) and low (RNEFC medium; *SI Appendix*, Table S3) Wnt conditions (*SI Appendix*, Fig. S3). Epithelial cells from both the embryonic FT and uterine tissues grew into organoids at a similar growth rate in the high Wnt culture medium. More importantly, these organoids appeared closer to adult mouse FT organoids, irrespective of the spatial origin of the epithelial cell types (*SI Appendix*, Figs. S3 and S4). In contrast, organoids cultured in low Wnt conditions from both embryonic tissues were comparable to adult mouse uterine organoids (*SI Appendix*, Figs. S3 and S4). Histological analysis confirmed that organoids cultured in high and low Wnt conditions were more akin to adult mouse FT and uterine organoids, respectively (Fig. 2*D* and *SI Appendix*, Figs. S3 and S4). Therefore, the region-specific role of Wnt signaling in the in vivo development of MDs is recapitulated in our robust culture system. In line with the temporal differences in the ontogeny of the female reproductive tract between mice and humans, mouse MD and neonatal reproductive tract epithelia express Pax8 and cytokeratin 8 (Ck8) but not AcTub (ciliated cells) and Foxa2 (expressed by the endometrial glands and secretory cells of the adult FT) (Fig. 2*E* and *SI Appendix*, Table S2). However, using our culture system, organoids cultured in both high and low Wnt conditions acquired the expression of AcTub and Foxa2 (Fig. 2 *F–I* and *SI Appendix*, Fig. S1), suggesting that our culture conditions allow for the self-renewal as well as the differentiation of MD epithelial cells. In summary, we have optimized a method of culturing MD organoids by modulating the levels of Wnt signaling.

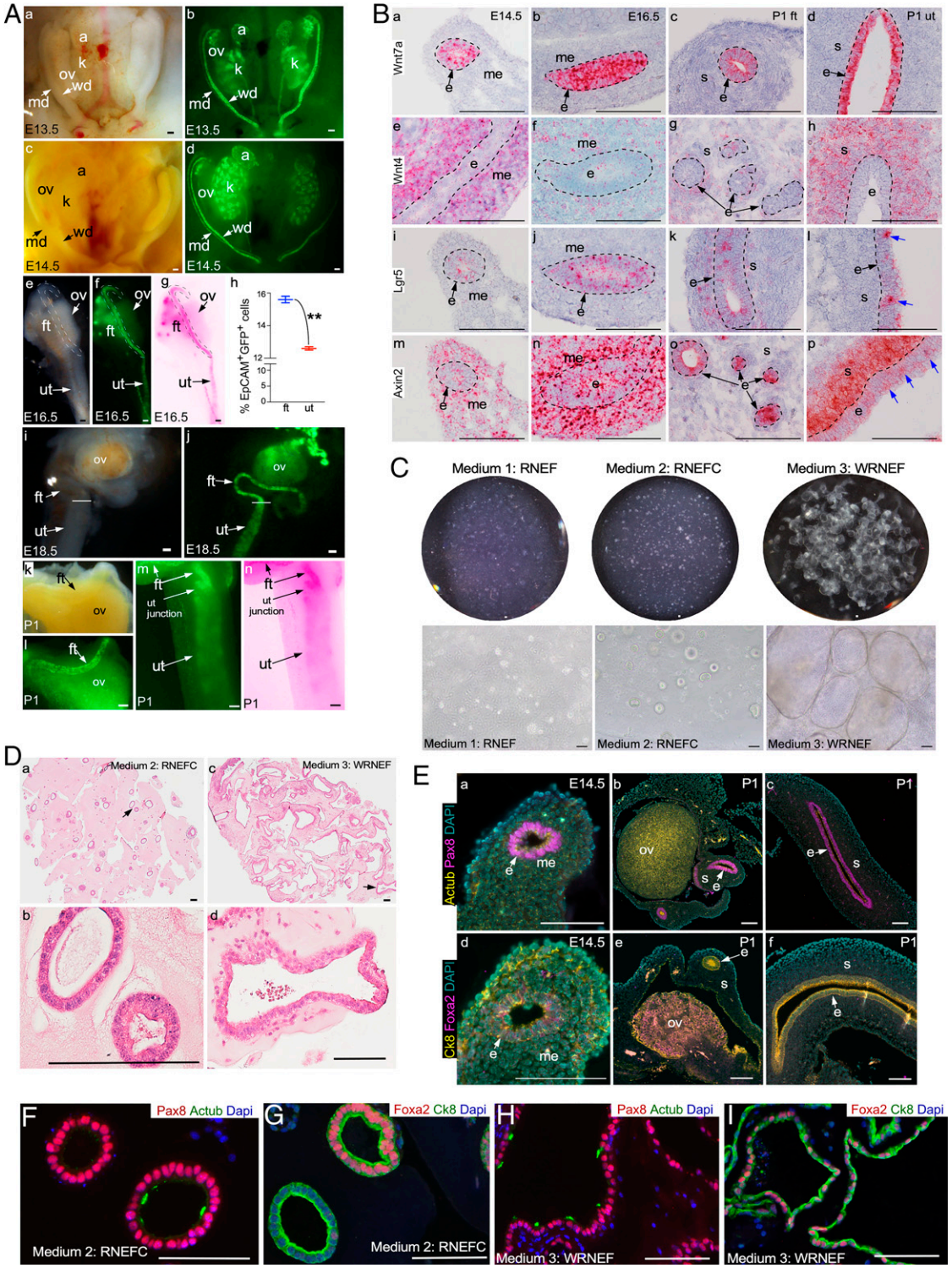

Fig. 2. Derivation of organoids from the mouse MD epithelium. (*A*) Gross bright-field (*A*, *a*, *c*, *e*, *i*, and *k*) and GFP fluorescence (*A*, *b*, *d*, *f*, *j*, *l*, and *m*) images and color-inverted (*A*, *g* and *n*) images of the female urogenital system collected from TCF-GFP mice at E13.5 (*A*, *a* and *b*), E14.5 (*A*, *c* and *d*), E.16.5 (*A*, *e*–*g*), E18.5 (*A*, *i* and *j*), and P1 (*A*, *k*–*n*) ($n = 5$ each stage), showing real-time Wnt activity marked by GFP expression. (*A*, *h*) Quantification of FACS-sorted EpCAM+ GFP+ from MDs collected from TCF-GFP mice at E16.5; $n = 6$; $^{**}P = 0.005$, unpaired *t* test with Welch's correction. Data represent means ± SEM. Dotted lines in *A*, *e*–*g* outline presumptive FTs. Transverse lines in *A*, *i* and *j* denote FTs and the uterotubular junction, respectively. (*B*) In situ hybridization for *Wnt7a* (*B*, *a*–*d*), *Wnt4* (*B*, *e*–*h*), *Lgr5* (*B*, *i*–*l*), and *Axin2* (*B*, *m*–*p*) messenger RNA in E14.5 (*B*, *a*, *e*, *i*, and *m*) and E16.5 (*B*, *b*, *f*, *j*, and *n*) MDs and P1 FTs (*B*, *c*, *g*, *k*, and *o*) and uteri (*B*, *d*, *h*, *l*, and *p*) ($n = 5$ biological replicates × 10 tissue sections per replicate). (*C*) Whole-well and representative images of organoids derived from E14.5 MD epithelial cells and cultured in RNEF or RNEFC and WRNEF ($n = 32$ MDs from 8 different dams). (*D*) Representative histological images of E14.5 MD epithelial cell–derived organoids cultured in RNEFC and WRNEF media. Arrows in *D*, *a* and *c* point to areas that are presented as higher-magnification images in *D*, *b* and *d*, respectively. (*E*) Coimmunostaining for Pax8 and Mouse AcTub (*E*, *a*–*c*) and Foxa2 and Ck8 (*E*, *d*–*f*) in E14.5 MDs (*E*, *a* and *d*) and P1 FTs (*E*, *b* and *e*) and uteri (*E*, *c* and *f*) ($n = 3$ biological replicates × 5 images per replicate). (*F*–*I*) Coimmunostaining for Pax8 and Actub (*F* and *H*) and Foxa2 and Ck8 (*G* and *I*) in organoids from *D* ($n = 3$ biological replicates × 5 images per replicate). a, adrenal glands; k, kidney; md, Müllerian duct; ut junction, uterotubular junction; wd, Wolffian duct. Data represent means ± SEM. (Scale bars, 100 μm unless indicated otherwise.)

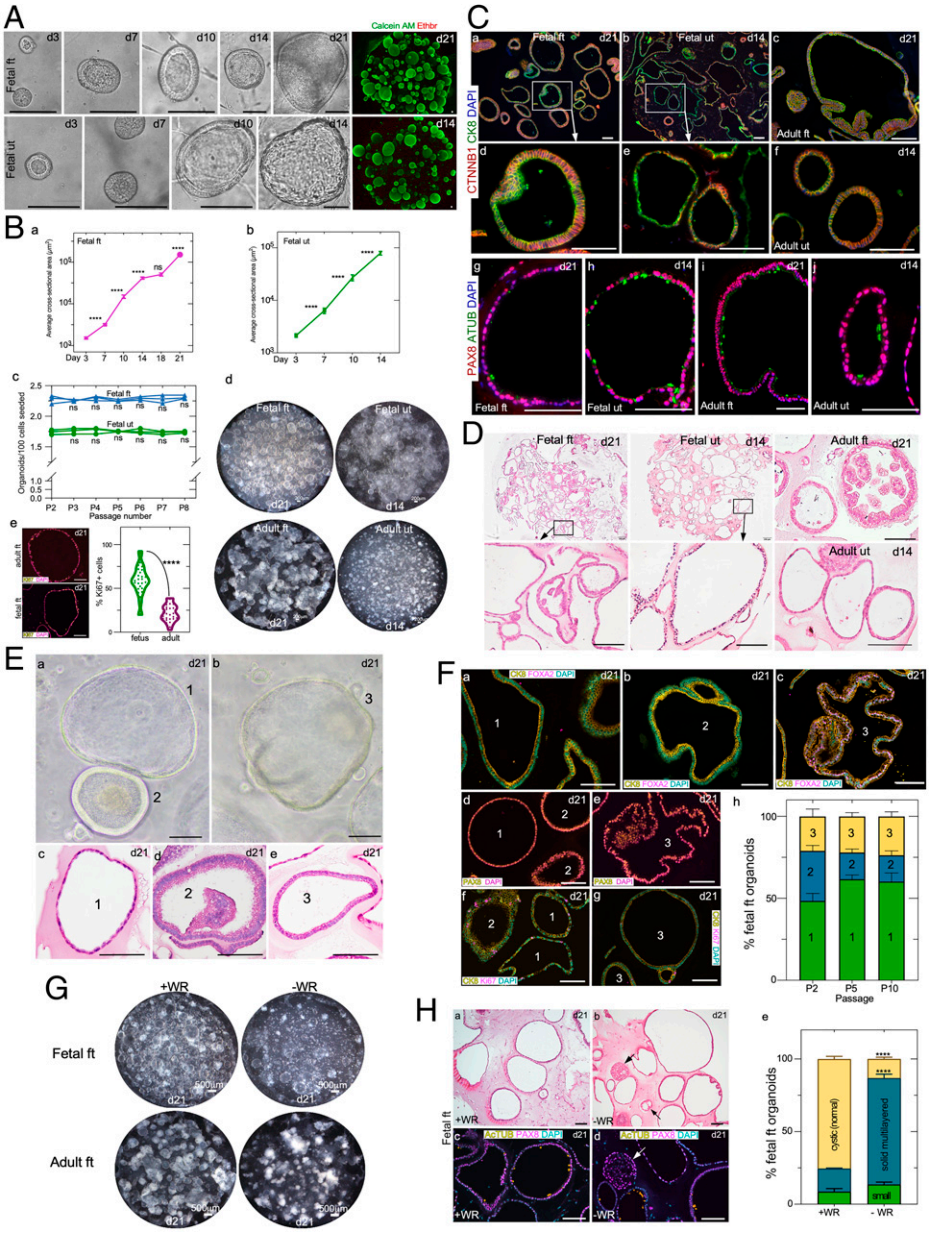

Fig. 3. Human fetal FT and uterine organoids and their comparison with adult tissue-derived organoids. (*A*) Timeline depicting organoid development of human fetal FT and uterine epithelial cells. Fluorescent images of fetal organoids after calcein AM (green) and ethidium homodimer 1 (red) cell-viability staining ($n = 5$). (*B*, *a* and *b*) Quantification of the average fetal FT (*B*, *a*) and uterine (*B*, *b*) organoid size at various days of culture; $n = 3$; ****$P =$ <0.0001; ns, not significant; Brown–Forsythe and Welch's ANOVA with Dunnett's T3 multiple-comparison test. (*B*, *c*) Quantification of the fetal organoid forming efficiency at the indicated passages; $n = 3$ each; two-way ANOVA with Sidak's test. (*B*, *d*) Whole-well bright-field images of fetal and adult FT and uterine organoids cultured in 24-well plates ($n = 3$ each). (*B*, *e*) Representative fluorescent images and quantification of Ki67+ proliferating cells in adult and fetal FT organoids; $n = 3$ biological replicates × 10 images per replicate; ****$P =$ <0.0001, unpaired *t* test with Welch's correction. (*C*) Coimmunostaining for β-catenin/CTNNB1 and CK8 (*C*, *a–f*) and PAX8 and AcTUB (*C*, *g–j*) in fetal FT (*C*, *a*, *d*, and *g*), fetal uterine (*C*, *b*, *e*, and *h*), adult FT (*C*, *c* and *i*), and adult uterine (*C*, *f* and *j*) organoids at the indicated days of culture ($n = 3$ biological replicates per group × 10 tissue sections of 5-μm thickness per replicate). *C*, *d* and *e* represent higher-magnification images of *C*, *a*, *Inset* and *C*, *b*, *Inset*, respectively. (*D*) Representative histological images of fetal and adult organoids ($n = 3$ each). (*D*, *Insets*) Higher-magnification images. (*E*) Representative gross (*E*, *a* and *b*) and histological images (*E*, *c–e*) of three different types of fetal organoids ($n = 3$ biological replicates each). (*F*) Coimmunostaining for CK8 with FOXA2 (*F*, *a–c*) and Ki67 (*F*, *f* and *g*) and immunostaining for PAX8 (*F*, *d* and *e*) in the three different types of fetal organoids from *E* at the indicated days of culture. Type 1 and 2 organoids were PAX8+ and FOXA2−, whereas type 3 organoids were positive for both markers. Quantification of the distribution of these three types of organoids at the indicated passages 2, 5, and 10; $n = 3$; two-way ANOVA with Tukey's multiple-comparison test. (*G*) Representative whole-well images of fetal and adult FT organoids cultured with or without WNT3a and R-Spondin-1 ($n = 3$ biological replicates per group). (*H*) Representative histological (*H*, *a* and *b*) and PAX8 and ACTUB–colabeled fluorescent (*H*, *c* and *d*) images of fetal FT organoids from *G*. Arrows in *H*, *b* and *d* denote small multilayered organoids present in Wnt-deficient (−WR) culture conditions. (*H*, *e*) Quantification of the distribution of different fetal FT organoid type cultures in high Wnt (+WR) and low Wnt (−WR) conditions; $n = 3$ biological replicates per group; ****$P =$ <0.0001, two-way ANOVA with Tukey's multiple-comparison test. Data represent means ± SEM. (Scale bars, 100 μm unless indicated otherwise.)

Human Fetal Reproductive Tract Organoids. We dissected primitive FTs and the uterus from the fetal reproductive tracts. The tissues were subjected to enzymatic digestion separately. The resulting single-cell suspensions were then plated in BME matrix droplets. We trialed four different medium compositions for culturing these cells. Two of them were the same as used for culturing mouse MD organoids (Fig. 2 and *SI Appendix*, Table S3). The other two medium compositions were previously described for growing adult FT (25% WRN CM, EGF) and uterine (25% WRN CM, EGF, FGF10) organoids and were adopted here to compare directly the intrinsic properties of fetal and adult organoids under similar culture conditions (*SI Appendix*, Table S3) (29–31). Our results demonstrated robust and comparable growth of fetal organoids in all four medium conditions (*SI Appendix*, Fig. S5) and therefore we decided to use the adult FT and uterine organoid media.

Fetal FT as well as uterine organoids showed robust growth and developed progressively from single cells in both these culture media (Fig. 3 *A* and *B*, *a* and *b*). To confirm the viability of these organoids, we performed calcein AM (green, marks viable cells) and ethidium homodimer-1 (red, stains dead cells) assays, which revealed the healthy growth of fetal organoids in our culture conditions (Fig. 3*A*). Importantly, the fetal organoids could be cultured repeatedly and maintained for more than eight passages, during which time their growth rates remained constant, indicating that our culture conditions support the long-term growth of these organoids (Fig. 3 *B*, *c*). Moreover, these fetal organoids could be cryopreserved and recovered successfully after thawing without affecting their growth and/or morphological characteristics (*SI Appendix*, Fig. S6*A*). Therefore, we report the establishment of culture conditions for the successful growth and long-term maintenance of human fetal reproductive tract organoids.

While both fetal and adult organoids express CK8 and β-catenin/CTNNB1, a marker of the adherens junction (32), confirming their epithelial nature (Fig. 3 *C*, *a–f*), they differ significantly from each other (Fig. 3 *C* and *D*). Grossly, fetal FT organoids showed cystic morphology compared with adult FT organoids, and only 20% of fetal organoids presented a solid appearance, typically observed in mature adult FT organoids due to epithelial folding and invaginations (Fig. 3 *B*, *d* and *D*). Fetal uterine organoids were much bigger, and their epithelium appeared slightly thinner compared with the adult uterine organoids (Fig. 3 *B*, *d* and *D*). Consistent with human fetal tissue (Fig. 1), fetal organoids had a higher number of Ki67+ proliferating cells than adult organoids (Fig. 3 *B*, *e*). Interestingly, while fetal and adult FT organoids expressed PAX8 and AcTUB similar to their in vivo tissue counterparts, fetal uterine organoids, unlike fetal uterine tissues, expressed AcTUB in addition to PAX8 (Fig. 3 *C*, *g–j*). This further highlights the robustness of our culture conditions that not only preserve the in vivo tissue characteristics but also promote the in vitro differentiation of immature fetal epithelium.

A closer examination of fetal FT and uterine organoids revealed three different kinds of organoids that coexisted in our cultures and were maintained throughout the passages (Fig. 3 *E* and *F*). Type 1 organoids consisted of a thin monolayer of epithelial cells (PAX8+ FOXA2−) lying in direct contact with the BME matrix. These appeared comparable to human adult intestinal spheroids, which are enriched for stem/progenitor cells, and mouse fetal intestinal spheroids (33–35). Type 2 organoids consisted of a pseudostratified epithelial cell layer (PAX8+ FOXA2−) with or without epithelial invaginations. Type 3 organoids were lined with a single layer of columnar epithelial cells (PAX8+ FOXA2+) (Fig. 3 *E* and *F*). All three types of fetal organoids had KI67+ proliferating cells (Fig. 3 *F*, *f* and *g*). These results suggest that type 1 organoids represent the undifferentiated immature nature of fetal epithelia, whereas type 2 and 3 organoids are more similar to adult tissue-derived organoids containing both differentiated and undifferentiated cells.

Wnt signaling is required for both self-renewal and differentiation of epithelial cells (23, 30). Therefore, we cultured fetal FT and uterine epithelial cells without WNT3a and R-spondin (WR) to investigate the impact of the Wnt signaling ablation on any or all three types of organoids. Compared with high Wnt conditions, adult FT organoids were smaller and appeared collapsed in the absence of WR, confirming the absolute requirement of Wnt signaling for the healthy growth of these organoids (Fig. 3*G*). In contrast, the majority of the type 1 fetal FT and uterine organoids continue to grow and maintain their cystic morphology in WR-deficient culture conditions (Fig. 3*G* and *SI Appendix*, Fig. S7). Type 2 and 3 organoids become smaller in size and acquire a solid multilayered morphology. These multilayered organoids had PAX8+ secretory cells but no AcTUB ciliated cells (Fig. 3 *H*, *c–e* and *SI Appendix*, Fig. S7), suggesting that the differentiation of these organoids is compromised in WNT-deficient conditions. Overall, we highlight the essential differences between fetal and adult organoids. Our established culture system preserves in vivo tissue characteristics that is evidenced by the characteristic behavior of fetal epithelium under varying Wnt conditions.

Proteomic Differences in Human Fetal and Adult Organoids. So far, our results indicate that human fetal and adult organoids differ significantly from each other. This prompted the in-depth investigation into the proteomic differences between these organoids. Therefore, we compared the relative protein abundance in fetal and adult organoids by quantitative mass spectrometry. Tryptic peptides from cultured human fetal and adult FT and uterine organoids were labeled with isobaric tags (iTRAQ 4plex labeling system) and were subsequently analyzed by liquid chromatography–tandem mass spectrometry (LC-MS/MS) (Fig. 4*A*). A combined total of 1,883 and 2,189 proteins with a strict false discovery rate <1% in FT and uterine groups, respectively, was detected by our proteomic analysis (Fig. 4 *B* and *C*). Quantitative LC-MS/MS results in these groups were then compared using Venn diagrams to identify the number of shared and differentially expressed proteins between the adult and fetal organoids in both the FT organoid group and the uterine organoid group (Fig. 4 *B* and *C*). A set of 1,122 proteins in the FT group and 1,599 proteins in the uterine group was identified to be commonly expressed between the adult and fetal organoids (Dataset S1). These proteins were then mapped using Perseus software to generate heatmaps highlighting the up- and down-regulated proteins in the FT and uterine groups (Fig. 4 *D* and *E*). As expected, the proteomes of fetal and adult organoids differed significantly from each other. Out of the numerous differentially expressed proteins, here we highlighted the top 10 up- and down-regulated proteins in the fetal organoids relative to the adult organoids (Fig. 4 *D* and *E*).

NEDD4, an E3 ubiquitin ligase, was up-regulated in the fetal FT organoids compared with the adult FT organoids (Fig. 4*D*). NEDD4 is a known modulator of Wnt signaling and controls proliferation and self-renewal of intestinal stem cells (36). Peroxiredoxin-4 (PRDX4) is an antioxidant protein that is highly enriched in human follicular fluid (37). Expectedly, PRDX4 was down-regulated in fetal FT organoids compared with the adult ones (Fig. 4*D*). In the case of the uterine group, fetal organoids showed up-regulated expression of H1-1/HIST1H1A and PPP1R26 (protein phosphatase 1 regulatory subunit 26), proteins involved in cell proliferation, compared with the adult organoids (Fig. 4*E*). On the other hand, CARMIL1 (capping protein regulator and myosin 1 linker 1), a protein that is widely expressed in the mature epithelia of tubular organs including endometrial glands (38), was consistently down-regulated in fetal uterine organoids compared with the adult ones, reflecting the immature nature of the fetal uterine epithelium (Fig. 4*E*). Next, we performed Ingenuity pathway analysis on the list of proteins significantly up-regulated in fetal and adult organoids (Fig. 4 *F–I*). Consistent with the highly proliferative nature of the fetal FT epithelium (Fig. 1), we detected key canonical pathways that are involved in cell growth and proliferation in the fetal FT organoids, including ERK/MAPK signaling ($-\log P = 2.37$), RAC signaling ($-\log P = 2.00$), cyclins and cell-cycle regulation ($-\log P = 1.76$), cell-cycle G1/S checkpoint regulation ($-\log P = 1.48$), and DNA methylation and transcriptional repression signaling ($-\log P = 1.40$) (Fig. 4*F*). At the same time, the mature differentiated nature of adult FT organoids was reflected by up-regulated retinoic acid–mediated apoptosis signaling ($-\log P = 1.46$) and epithelial adherens junction signaling ($-\log P = 1.33$) pathways in these organoids (Fig. 4*G*). Pathways involved in metabolism and cell proliferation were detected in fetal uterine organoids (Fig. 4*H*). Receptor tyrosine kinase (RTK) signaling being essential for endometrial functions, the top five pathways belonging to the RTK family were detected in adult uterine organoids (Fig. 4*I*). Thus, these proteomic data highlight the major differences in the protein expression and the signaling pathways between the fetal and adult organoids.

In Vitro Transplantation and Regeneration of Decellularized Adult Tissues by Fetal Organoids. Defects of the reproductive tract organs in patients with MDAs are currently surgically

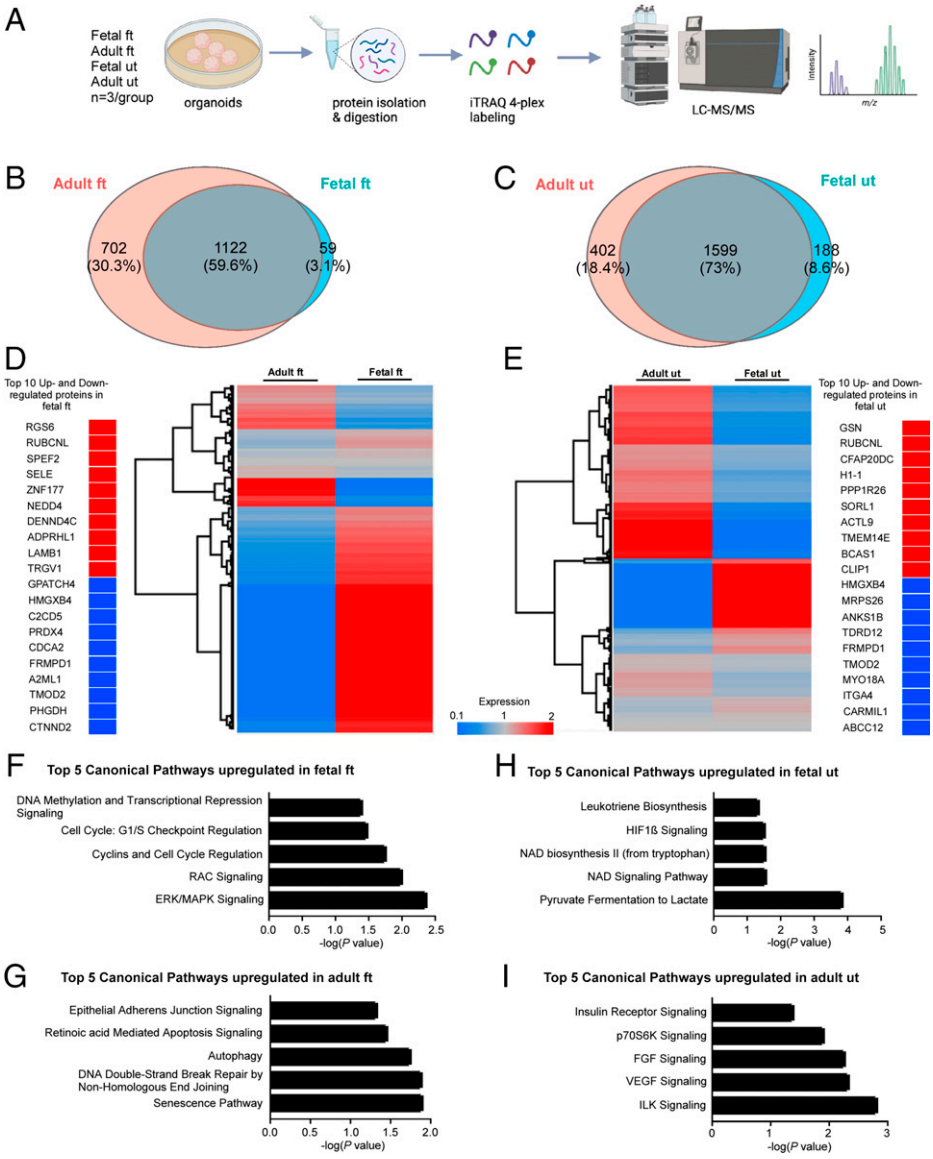

Fig. 4. Proteomic profiling of fetal and adult FTs and uterine organoids. (*A*) A pictorial outline of the experimental schedule used in *B*–*I*. Organoids from human fetal and adult FTs and uterus ($n = 3$ biological replicates in each group) were subjected to protein extraction and digestion. Following tryptic digestion, peptides of each sample were labeled with iTRAQ 4plex prior to LC-MS/MS analysis. (*B* and *C*) Venn diagrams depicting the number of common and differentially expressed proteins in fetal and adult FT (*B*) and uterine organoids (*C*). LC-MS/MS analysis detected a total of 1,181 proteins in the fetal FT organoids, 1,824 proteins in the adult FT organoids, 1,787 proteins in the fetal uterine organoids, and 2,001 proteins in the adult uterine organoids with a false discovery rate <1%. (*D* and *E*) Hierarchical clustering analysis of the expression levels of 1,122 proteins commonly expressed in adult and fetal FT organoids and 1,599 proteins commonly expressed in adult and fetal uterine organoids. Clustering highlighted the top 10 up-regulated (>1.5-fold) and down-regulated (<0.66-fold) expressed proteins in fetal FT (*D*) and uterine organoid (*E*) groups. (*F*–*I*) Ingenuity pathway analysis of LC-MS/MS data from *A* depicting the top 5 significantly up-regulated pathways in the indicated organoid groups. The *x* axis indicates Fisher's exact test *P* value, while the *y* axis represents the corresponding canonical pathways.

repaired using tissue grafts from other organs, such as skin and omentum (39, 40). To assess the differentiation potential of the immature epithelia of fetal organoids and to test if such organoids that are grown and expanded in laboratory conditions can repair and regenerate reproductive organs in these patients, we transplanted fetal organoids onto decellularized scaffolds derived from patients undergoing bilateral salpingectomy and total hysterectomy (Fig. 5*A*). Therefore, we obtained small punch biopsies (5 to 10 mm) representing the fimbrial end of adult human FT and the endometrium of the adult human uterus. Five thousand cells derived from the fetal FT and uterine organoids were then plated on top of these decellularized scaffolds of the respective organs. At least two approaches, including culture conditions in which Notch signaling is inhibited by γ-secretase inhibitors (30, 41) and one in which cells are cultured at the air–liquid interface (ALI) (42), have been shown to promote the differentiation of adult FT and uterine epithelium. Therefore, we incorporated both these approaches along with the conventional submerged cell-culture method in our protocols to promote the differentiation of fetal cells during the recellularization of the decellularized scaffolds (Fig. 5 *B*–*E*). After 21 d in culture, seeded fetal epithelial cells had engrafted on the surface of the decellularized scaffolds in all three culture conditions and appeared as a continuous transparent rim of cells lining these scaffolds. As expected, controls represented by the decellularized scaffolds that were cultured in the absence of cells did not present with such a transparent rim of cells on their surfaces (Fig. 5 *B*–*E*). More importantly, histological analysis not only confirmed that the fetal FT epithelial cells had recellularized the adult FT scaffolds in all three conditions (Fig. 5 *F*–*I*) but also revealed that the engrafted cells formed epithelial clefts, were actively proliferating, and differentiated into secretory and ciliated cell lineages. Similarly, engrafted fetal uterine epithelial cells regenerated both the luminal and glandular epithelia of the adult uterine scaffolds, were actively proliferating, and differentiated into the uterine secretory and ciliated cell lineages (Fig. 5 *J*–*M*). In contrast, control scaffolds showed no traces of hematoxylin-stained nuclei, further confirming the complete decellularization of the original punch biopsies (Fig. 5 *F* and *J*). Interestingly, the epithelial lining of the scaffolds cultured in the presence of DAPT (a γ-secretase inhibitor) and under ALI conditions appeared more mature and differentiated than the scaffolds cultured under conventional submerged conditions (Fig. 5 *G*–*I*).

As mentioned above, engrafted cells in all the recellularized scaffolds expressed PAX8 (secretory cells), AcTUB (ciliated cells),

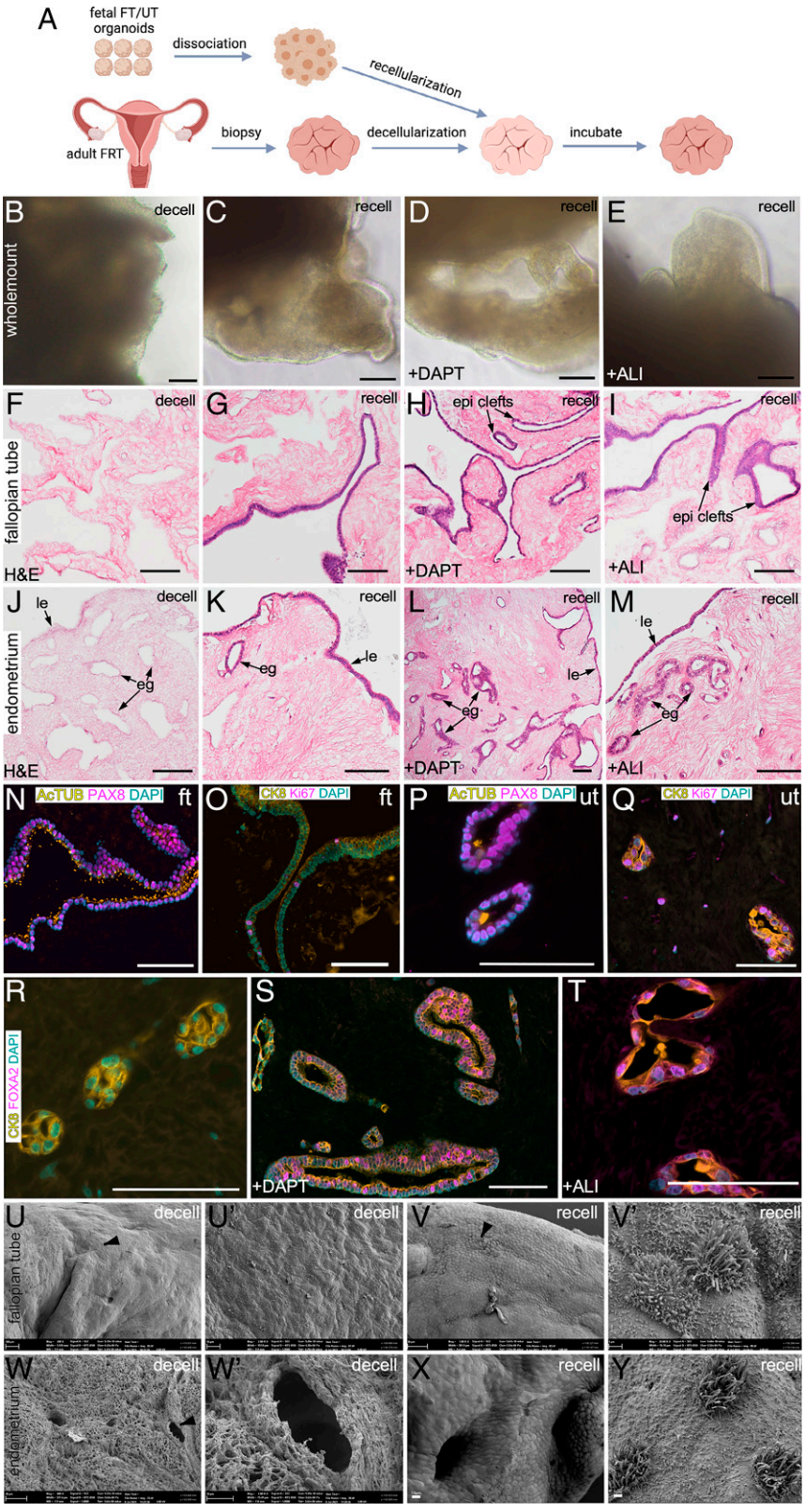

Fig. 5. Transplantation of human fetal organoids onto decellularized adult tissue scaffolds leads to epithelial regeneration. (*A*) Schematic showing the experimental schedule used in *B*–*Y*. FRT, female reproductive tract. (*B*–*E*) Representative whole-mount bright-field images of decellularized (decell) (*B*) and recellularized (recell) (*C*–*E*) adult tissue scaffolds cultured in the presence of vehicle (*C*) or DAPT (*D*) or at an ALI (*E*) (n = 3 per group). (*F*–*M*) Representative histological images of adult FT (*F*–*I*) and uterine (*J*–*M*) tissue-derived scaffolds before (*F* and *J*) and after (*G*–*I* and *K*–*M*) fetal cell transplantation. Scaffolds were cultured in the presence of vehicle (*G* and *K*) or DAPT (*H* and *L*) or at an ALI (*I* and *M*) (n = 3 per group × 10 tissue sections of 5-μm thickness were examined per replicate). (*N*–Q) Coimmunostaining for PAX8 (secretory cells) and AcTUB (ciliated cells) (*N* and *P*) and Ki67 (proliferating cells) and CK8 (epithelial cells) (*O* and *Q*) in recellularized FT (*N* and *O*) and uterine (*P* and *Q*) scaffolds. (*R*–*T*) Coimmunostaining for FOXA2 and CK8 in recellularized uterine scaffolds cultured in the presence of vehicle (*R*) or DAPT (*S*) or at an ALI (*T*); n = 3 biological replicates per group × 5 tissue sections of 5-μm thickness were stained per replicate. Scanning electron microscopy of decellularized (*U*, *U*′, *W*, and *W*′) and recellularized (*V*, *V*′, *X*, and *Y*) FT (*U*, *U*′, *V*, and *V*′) and uterine (*W*, *W*′, *X*, and *Y*) scaffolds (n = 3 per group). The epithelial cell layer consisting of an admix of ciliated and secretory cells was present after but not before recellularization. *U*′, *V*′, and *W*′ represent high-magnification images of areas marked by arrowheads in *U*, *V*, and *W*, respectively. Epi clefts, epithelial clefts. (Scale bars, 100 μm unless indicated otherwise.)

and KI67 (proliferating cells), suggesting that these fetal-derived cells adapt to their native tissue-derived scaffolds and differentiate appropriately into the constituent secretory and ciliated cell types (Fig. 5 *N*–*Q*). FOXA2 expression confirmed the presence of mature endometrial glands in scaffolds belonging to the DAPT and ALI groups (Fig. 5 *S* and *T*). However, very weak or no FOXA2 staining was detected in uterine scaffolds cultured under conventional submerged conditions (Fig. 5*R*), suggesting the primitive nature of glands in these scaffolds. For further confirmation of the efficient decellularization and recellularization processes, we performed scanning electron microscopy of all the scaffolds (Fig. 5 *U*–*Y*). As expected, decellularized FT as well as uterine scaffolds were completely devoid of epithelial cells. Interestingly, these scaffolds had preserved the typical anatomical features of their respective organs, such as folds/clefts in the FTs and glands in the uterus (Fig. 5 *U*, *U*′, *W*, and *W*′), suggesting that

our decellularization protocol efficiently removed cellular components of these organs without damaging the anatomy of the acellular extracellular matrix. In contrast, surfaces of the recellularized scaffolds were perfectly lined by the transplanted epithelial cells that consisted of an admix of nonciliated and ciliated cells (Fig. 5 *V*, *V′*, *X*, and *Y*). To test the applicability of our in vitro transplantation assay for adult tissue-derived organoids, we cultured 5,000 cells derived from adult human FT and uterine organoids on adult tissue-derived decellularized scaffolds under ALI conditions (*SI Appendix*, Fig. S8). Histological analysis confirmed robust growth of both adult FT and uterine epithelium on these scaffolds after 21 d of the incubation period (*SI Appendix*, Fig. S8). We observed that the recellularization efficiency of the adult organoids was less than that of the fetal organoids, which is probably a reflection of the differences in the proliferation rate of adult and fetal epithelium (Fig. 3 *B*, *e*).

The female reproductive tract epithelium is highly responsive to ovarian hormones (43). Estrogen drives the proliferation of reproductive tract epithelial cells mainly through estrogen receptor alpha (ESR1) (43). To test if the fetal cells that recellularized scaffolds are responsive to estrogen, we examined the expression of ESR1 and a phosphorylated form of ESR1 (pSer118-ESR1) (*SI Appendix*, Fig. S9). Consistent with a previous study (44), ESR1 and pSer118-ESR1 were present in both epithelial and stromal cells of adult mouse uterus (*SI Appendix*, Fig. S9). Therefore, we used mouse uterine tissue as a positive control for immunostaining for these two markers. We observed a robust expression of ESR1 and pSer118-ESR1 in the recellularized scaffolds (*SI Appendix*, Fig. S9), suggesting the hormone-responsive nature of recellularized epithelia.

Next, to investigate if fetal epithelial cells upon transplantation were appropriately differentiated and gave rise to fully functional ciliated cells, we analyzed the cells to identify their different stages of ciliation (*SI Appendix*, Fig. S10). Forkhead box protein J1 (FOXJ1) is expressed in epithelial cells committed to ciliation, including cells that have yet to acquire cilia (45). Radial spoke head component 4A (RSPH4A) is a component of the radial spoke head assembly of motile cilia, and its expression is limited to differentiated ciliated cells (46, 47). The coiled-coil domain containing 39 (CCDC39) protein is involved in the assembly of inner dynein arms and the dynein regulatory complex required for normal ciliary motility (48). CCDC39 specifically marks a subset of ciliated cells with motile cilia (48). Using these three markers, we were able to locate epithelial cells committed to ciliation (FOXJ1), differentiated ciliated cells (RSPH4A), and ciliated cells with motile cilia (CCDC39) in adult human FTs (*SI Appendix*, Fig. S10 *A*, *a*–*c*). Our analysis of publicly available single-cell RNA-sequencing data of adult human endometrium revealed that these three markers also correctly identify the ciliated cells in human endometrium (*SI Appendix*, Fig. S10*B*) (49). Therefore, we performed immunostaining for FOXJ1, RSPH4A, and CCDC39 on scaffolds recellularized with human fetal FT and uterine epithelial cells and were able to decipher the presence of differentiated ciliated cells, including cells with motile cilia marked by CCDC39, in these scaffolds (*SI Appendix*, Fig. S10 *A*, *d*–*i*). Collectively, these data provide evidence that the fetal organoids comprising the immature epithelial progenitors represent a transplantable source of cells and have the capacity to differentiate in vitro and regenerate the adult organs.

Effects of the Suppression of Wnt Signaling on Human and Mouse Fetal Epithelium. Defective Wnt signaling is associated with human MDAs (7, 8). Here, we utilized our scaffold model to understand the functional consequences of the Wnt signaling suppression in the human fetal epithelium (Fig. 6*A*). Fetal FT organoids were transplanted on decellularized adult FT scaffolds and were then treated with either PKF118-310, a Wnt signaling inhibitor (50), or vehicle. While in the vehicle-treated group, we observed normal recellularization of scaffolds with the proliferating epithelial cells (CK8+ KI67+) (Fig. 6 *B* and *C*), PKF118-310 treatment completely suppressed the engraftment and the subsequent growth of fetal epithelial cells on the scaffolds (Fig. 6 *D* and *E*). Next, we determined if a similar phenotype can be obtained in vivo in mice upon the deletion of the β-catenin (*Ctnnb1*) gene in their MD epithelium (Fig. 6 *F*–*V*). We have previously established a mouse model in which β-catenin deletion in the presence of doxycycline in the MD epithelium is driven by the Pax8 promoter (*Pax8*^{rtTA}*; tetO*^{Cre}*; Ctnnb1*$^{fl/fl}$) (26, 51). *Pax8*^{rtTA}*; tetO*^{Cre}*; Ctnnb1*$^{fl/fl}$ mice are referred to as *Ctnnb1*$^{fl/fl}$ before doxycycline treatment and *Ctnnb1*$^{\Delta/\Delta}$ after the treatment. *Ctnnb1*$^{fl/fl}$ mice were administered doxycycline from 13.5 d postcoitus to P21, and tissue samples were collected at regular intervals. We chose to delete β-catenin from the epithelial layer specifically at E13.5 because MD elongation is complete by this stage of mouse fetal development (52). Gross examination revealed intact MD epithelium which was confirmed by whole-mount Ck8 staining in both the control and mutant fetuses at E16.5 (Fig. 6 *F*–*I*). However, histologically, mutant MD epithelium appeared slightly disorganized compared with controls (Fig. 6 *J* and *K*). Immunostaining of β-catenin and Ck8 confirmed epithelium-specific loss of β-catenin in mutant but not in control mice (Fig. 6 *L* and *M*). At P3, compared with *Ctnnb1*$^{fl/fl}$ mice, uteri in *Ctnnb1*$^{\Delta/\Delta}$ mice are septate (Fig. 6 *N* and *O*). Histological analysis revealed that the mutant epithelium was underdeveloped and abnormal in mutants compared with controls (Fig. 6 *P* and *Q*). At P21, similar to MRKH patients (53), FTs in mutant mice were missing and the uterus presented a hypoplastic morphology (Fig. 6 *R* and *S*). Histological analysis confirmed that some uterine segments were devoid of epithelium, and only mesenchymal cells with no visible lumen were present (Fig. 6*U*). In some focal regions of the mutant uteri, a very thin and cystic epithelium was observed (Fig. 6*V*). In comparison, control uteri had normal luminal and glandular epithelia with the appropriate differentiation of mesenchymal compartments (Fig. 6*T*). Collectively, these data highlight the requirement of Wnt/β-catenin signaling in governing the self-renewal and differentiation of the fetal epithelium.

Discussion

The development of human MDs starts in a 5- to 6-wk-old fetus as aggregations and invaginations of coelomic epithelial cells (54). These cells continue to grow and migrate using the adjacent WDs as a guide (5). In males, MDs undergo regression soon after their formation under the influence of anti–Müllerian hormone (also known as Müllerian inhibiting substance) secreted by the Sertoli cells of the developing testis (4, 5), while in females, these ducts progressively differentiate and acquire organ-specific features of FTs, uterus, cervix, and the upper part of the vagina (54). In humans, midline fusion of MDs results in the formation of a uterovaginal canal, and the cranial part of this structure gives rise to the uterus by 9 to 10 wk of fetal age (54). By 16 wk of gestation, the caudal end of the uterovaginal canal starts acquiring features of the cervix, and the cervical glands are present at the age of 18 wk (17). This study has developed organoids from the female reproductive tract epithelium collected from fetuses between 9 and 14 wk of age. We get robust development of organoids representing the epithelium of FTs and the uterus. However, we did

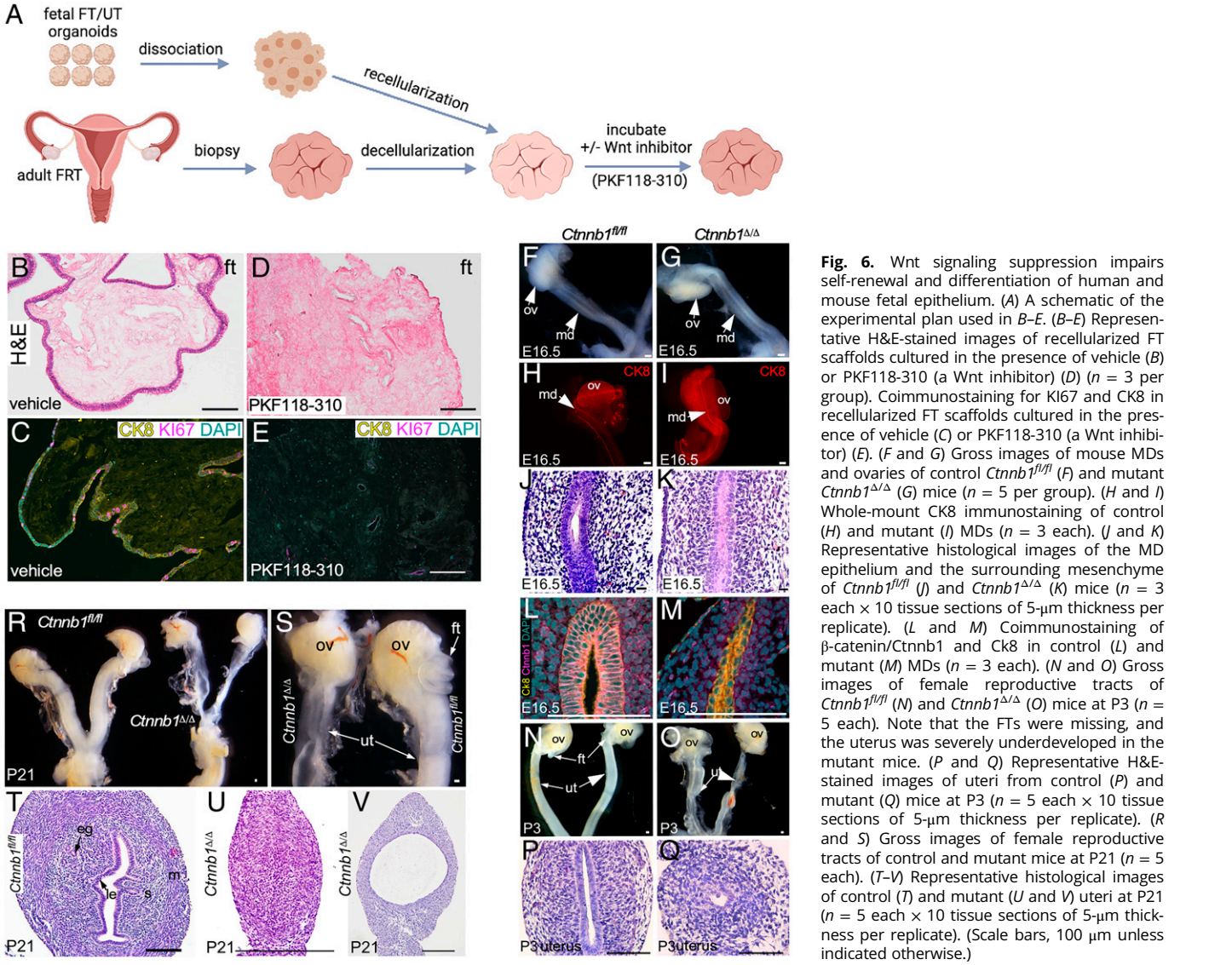

Fig. 6. Wnt signaling suppression impairs self-renewal and differentiation of human and mouse fetal epithelium. (*A*) A schematic of the experimental plan used in *B*–*E*. (*B*–*E*) Representative H&E-stained images of recellularized FT scaffolds cultured in the presence of vehicle (*B*) or PKF118-310 (a Wnt inhibitor) (*D*) (n = 3 per group). Coimmunostaining for KI67 and CK8 in recellularized FT scaffolds cultured in the presence of vehicle (*C*) or PKF118-310 (a Wnt inhibitor) (*E*). (*F* and *G*) Gross images of mouse MDs and ovaries of control *Ctnnb1*$^{fl/fl}$ (*F*) and mutant *Ctnnb1*$^{\Delta/\Delta}$ (*G*) mice (n = 5 per group). (*H* and *I*) Whole-mount CK8 immunostaining of control (*H*) and mutant (*I*) MDs (n = 3 each). (*J* and *K*) Representative histological images of the MD epithelium and the surrounding mesenchyme of *Ctnnb1*$^{fl/fl}$ (*J*) and *Ctnnb1*$^{\Delta/\Delta}$ (*K*) mice (n = 3 each × 10 tissue sections of 5-μm thickness per replicate). (*L* and *M*) Coimmunostaining of β-catenin/Ctnnb1 and Ck8 in control (*L*) and mutant (*M*) MDs (n = 3 each). (*N* and *O*) Gross images of female reproductive tracts of *Ctnnb1*$^{fl/fl}$ (*N*) and *Ctnnb1*$^{\Delta/\Delta}$ (*O*) mice at P3 (n = 5 each). Note that the FTs were missing, and the uterus was severely underdeveloped in the mutant mice. (*P* and *Q*) Representative H&E-stained images of uteri from control (*P*) and mutant (*Q*) mice at P3 (n = 5 each × 10 tissue sections of 5-μm thickness per replicate). (*R* and *S*) Gross images of female reproductive tracts of control and mutant mice at P21 (n = 5 each). (*T*–*V*) Representative histological images of control (*T*) and mutant (*U* and *V*) uteri at P21 (n = 5 each × 10 tissue sections of 5-μm thickness per replicate). (Scale bars, 100 μm unless indicated otherwise.)

not observe organoids with typical characteristics of cervical and vaginal epithelium in any of our cultures, even after culturing fetal epithelial cells in media described for growing adult cervical and vaginal organoids (55, 56). This means our culture methods accurately capture the developmental stages of the female reproductive tract organs, as our fetal tissue collections are limited to 9 to 14 wk of gestation. Cervix and vaginal development occur outside our tissue collection window and start around 16 wk of age. Unfortunately, we are unable to access fetal tissues beyond 14 wk of gestation. Additionally, due to the physical nature of the elective termination procedure, we can only recover intact female reproductive tracts in less than 10% of our collections, which severely limits the availability of the initial material required for various other experimental protocols.

MDAs are relatively common in infertile women compared with fertile women (1). Patients with MDAs are presented in the clinic with wide-ranging gynecological and obstetrical issues from menstrual disorders to infertility and recurrent first-semester miscarriages (1). The management of these patients depends on the anatomical defects, and the majority of patients are able to achieve reasonable sexual functions after the surgical management of the defects (57). Women with vaginal agenesis undergo vaginoplasty to create a neovagina (39). This surgical procedure involves inserting a skin graft, usually taken from the buttocks, attached to a prosthesis between the bladder and the rectum (39). Sometimes tissue grafts from other sites, such as human amnion and buccal mucosa, are also used for creating a neovagina (57, 58). Almost 90% of patients with MDAs have rudimentary Müllerian structures (57). However, our inability to culture and expand these tiny primitive Müllerian tissues is a major roadblock in using the native tissues for regenerative treatments of these patients. In this study, we have optimized the methodology for growing and expanding organoids from very small fetal tissues. We have also provided evidence that the transplantation of these organoids leads to the regeneration of decellularized adult tissue scaffolds. Given that decellularized scaffolds from human and animal tissues are approved by the Food and Drug Administration for human use (59), it is reasonable to think that Müllerian organoids integrated with decellularized or biosynthetic scaffolds would be a superior alternative to the current surgical reconstruction approaches for MDA patients. There is a strong precedent for implementing such a surgical approach, because a bovine dermal collagen-derived scaffold has already been successfully used in an MRKH patient to create a neovagina (60).

Studies on human organ development are often limited due to the restricted availability of fetal tissues. Gene sequencing of patients with MDAs has identified many genes reflecting the diverse array of phenotypes observed in these patients (1).

However, there are limited functional validation studies of these genetic alterations and their association with MDAs. The majority of the evidence for their involvement in the pathogenesis of MDAs comes from genetically modified mouse models (5). For example, defects in *WNT4*, *PAX2*, and *LHX1/LIM1* genes are observed in women with MDAs, and the deletion of these respective genes in mouse models has also shown defects in MD development and differentiation (5). There are several key differences in human and mouse reproductive tracts that limit the utility of these models to fully understand MDAs (54). In humans, MDs undergo extensive midline fusion resulting in the formation of a uterovaginal canal and paired FTs (54). The uterovaginal canal undergoes extensive remodeling, including the regression of the midline septum, and gives rise to the uterus, cervix, and upper vagina (54). The retention of midline septa results in the development of the septate uterus, which is the most common structural abnormality observed in human MDAs (3). In contrast, mouse MDs undergo limited fusion toward the caudal end, and most of the MDs remain unfused, giving rise to two uterine horns and two FTs (61). Therefore, mouse models have a limited potential in phenocopying the changes leading to the development of human septate uterus. We believe human fetal organoids combined with various tissue scaffolding techniques would spur the development of new models to investigate MDAs. Additionally, fetal organoids would also allow the rapid screening of numerous genetic defects identified in human patients with MDAs.

Epithelial–mesenchymal interactions play a significant role in the organogenesis of MDs and their subsequent differentiation to the female reproductive tract organs (62). The reciprocal cross-talk between these cellular compartments is essential for epithelial development, mesenchymal differentiation, and hormone responsiveness of the reproductive tract epithelia (62, 63). Studies using tissue recombinant models have demonstrated the requirement of stromal signals in functional differentiation of neonatal MD epithelium to uterine and vaginal epithelia (64). Cell type–specific genetic ablation studies have revealed that the loss of key developmental signals, such as WNT signaling, either in the epithelium or stromal cells, leads to abnormalities in nontargeted neighboring cells. For example, epithelial-specific deletion of *Wnt7a* results in abnormal mesenchymal differentiation of the mouse female reproductive tract organs by negatively affecting stromal Hoxa10 and Hoxa11 expression (65). Similarly, mesenchymal cell–specific loss of *Ctnnb1* in mice leads to severe defects in the adjacent epithelial compartment of female reproductive organs (15, 66). Although most organoids are grown from epithelial cells, recent studies have incorporated stromal and immune cells in organoid models for developing more holistic models to study human organ development and diseases (67–69). This study focused on human MD epithelial cells for organoid development. In future investigations, there is a need to incorporate stromal, endothelial, and immune cells in our organoid models to understand how paracrine and endocrine signals shape MD epithelial development and differentiation.

In summary, we have established and characterized human and mouse fetal FT and uterine organoids and performed a comparative analysis with their adult counterparts. We showed that these organoids could be expanded in vitro and can regenerate adult tissues upon transplantation. Fetal organoids can grow without the external supplementation of Wnt ligands and are proteomically different from adult organoids.

Materials and Methods

Human Fetal and Adult Organoids. Our full study protocol involving human subjects was approved by The University of Newcastle Human Ethics Committee and complied with Australia's National Health and Medical Research Council (NHMRC) National Statement on Ethical Conduct in Human Research regulations. Written consent was obtained from all donors. A detailed procedure relating to human fetal tissue collections is described by us in ref. 70. Details are in *SI Appendix*.

Data Availability. The mass spectrometry data reported in this article have been deposited in MassIVE (accession no. MSV000088200, see *SI Appendix* for login) (71). All other study data are included in the article and/or supporting information.

ACKNOWLEDGMENTS. We thank Dr. Shafiq Syed, Dr. Arnab Ghosh, Dr. Manish Kumar, Isabella Moore, and Sathish Indirathankam for technical assistance, and Dr. Huiming Zhang, Yun Lin, and Nicole Cole at the Analytical and Biomolecular Research Facility for help with scanning electron microscopy and FACS. This work is in part supported by funding from the NHMRC, Cancer Australia (1187542), and Ovarian Cancer Research Foundation. Some parts of experimental outlines presented in figures were created using BioRender.

Author affiliations: [a]School of Biomedical Sciences and Pharmacy, University of Newcastle, Callaghan, NSW 2308, Australia; [b]Cancer Detection and Therapy Research Program, Hunter Medical Research Institute, New Lambton Heights, NSW 2305, Australia; [c]Global Innovative Center for Advanced Nanomaterials, School of Engineering, University of Newcastle, Callaghan, NSW 2308, Australia; [d]Hunter New England Centre for Gynaecological Cancer, John Hunter Hospital, New Lambton Heights, NSW 2305, Australia; and [e]Department of Maternity and Gynaecology, John Hunter Hospital, New Lambton Heights, NSW 2305, Australia

1. L. Santana González, M. Artibani, A. A. Ahmed, Studying Müllerian duct anomalies–From cataloguing phenotypes to discovering causation. *Dis. Model. Mech.* **14**, dmm047977 (2021).
2. P. Acién, Incidence of Müllerian defects in fertile and infertile women. *Hum. Reprod.* **12**, 1372–1376 (1997).
3. F. Raga *et al.*, Reproductive impact of congenital Müllerian anomalies. *Hum. Reprod.* **12**, 2277–2281 (1997).
4. D. T. MacLaughlin, J. Teixeira, P. K. Donahoe, Perspective: Reproductive tract development–New discoveries and future directions. *Endocrinology* **142**, 2167–2172 (2001).
5. R. D. Mullen, R. R. Behringer, Molecular genetics of Müllerian duct formation, regression and differentiation. *Sex Dev.* **8**, 281–296 (2014).
6. D. H. Castrillon, "Development and maldevelopment of the female reproductive system" in *Gynecologic and Obstetric Pathology*, W. Zheng, O. Fadare, C. Quick, D. Shen, D. Guo, Eds. (Springer, Singapore, 2019), vol. **1**, pp. 1–40.
7. B. Backhouse *et al.*, Identification of candidate genes for Mayer-Rokitansky-Küster-Hauser syndrome using genomic approaches. *Sex Dev.* **13**, 26–34 (2019).
8. A. Biason-Lauber, D. Konrad, F. Navratil, E. J. Schoenle, A WNT4 mutation associated with Müllerian-duct regression and virilization in a 46,XX woman. *N. Engl. J. Med.* **351**, 792–798 (2004).
9. G. St-Jean *et al.*, Targeted ablation of Wnt4 and Wnt5a in Müllerian duct mesenchyme impedes endometrial gland development and causes partial Müllerian agenesis. *Biol. Reprod.* **100**, 49–60 (2019).
10. P. S. Tanwar *et al.*, Focal Mullerian duct retention in male mice with constitutively activated beta-catenin expression in the Mullerian duct mesenchyme. *Proc. Natl. Acad. Sci. U.S.A.* **107**, 16142–16147 (2010).
11. R. Prunskaite-Hyyryläinen *et al.*, Wnt4 coordinates directional cell migration and extension of the Müllerian duct essential for ontogenesis of the female reproductive tract. *Hum. Mol. Genet.* **25**, 1059–1073 (2016).
12. T. J. Carroll, J. S. Park, S. Hayashi, A. Majumdar, A. P. McMahon, Wnt9b plays a central role in the regulation of mesenchymal to epithelial transitions underlying organogenesis of the mammalian urogenital system. *Dev. Cell* **9**, 283–292 (2005).
13. A. Kobayashi *et al.*, β-catenin is essential for Müllerian duct regression during male sexual differentiation. *Development* **138**, 1967–1975 (2011).
14. N. A. Arango *et al.*, Conditional deletion of beta-catenin in the mesenchyme of the developing mouse uterus results in a switch to adipogenesis in the myometrium. *Dev. Biol.* **288**, 276–283 (2005).
15. E. Deutscher, H. Hung-Chang Yao, Essential roles of mesenchyme-derived beta-catenin in mouse Müllerian duct morphogenesis. *Dev. Biol.* **307**, 227–236 (2007).
16. T. E. Spencer, A. M. Kelleher, F. F. Bartol, Development and function of uterine glands in domestic animals. *Annu. Rev. Anim. Biosci.* **7**, 125–147 (2019).
17. S. J. Robboy, T. Kurita, L. Baskin, G. R. Cunha, New insights into human female reproductive tract development. *Differentiation* **97**, 9–22 (2017).
18. M. Habiba, R. Heyn, P. Bianchi, I. Brosens, G. Benagiano, The development of the human uterus: Morphogenesis to menarche. *Hum. Reprod. Update* **27**, 1–26 (2021).
19. G. Rossi, A. Manfrin, M. P. Lutolf, Progress and potential in organoid research. *Nat. Rev. Genet.* **19**, 671–687 (2018).
20. L. Meran *et al.*, Engineering transplantable jejunal mucosal grafts using patient-derived organoids from children with intestinal failure. *Nat. Med.* **26**, 1593–1601 (2020).

21. A. Singh, H. M. Poling, J. R. Spence, J. M. Wells, M. A. Helmrath, Gastrointestinal organoids: A next-generation tool for modeling human development. *Am. J. Physiol. Gastrointest. Liver Physiol.* **319**, G375–G381 (2020).
22. R. Heremans, Z. Jan, D. Timmerman, H. Vankelecom, Organoids of the female reproductive tract: Innovative tools to study desired to unwelcome processes. *Front. Cell Dev. Biol.* **9**, 661472 (2021).
23. A. Ghosh, S. M. Syed, P. S. Tanwar, In vivo genetic cell lineage tracing reveals that oviductal secretory cells self-renew and give rise to ciliated cells. *Development* **144**, 3031–3041 (2017).
24. L. Ariza, R. Carmona, A. Cañete, E. Cano, R. Muñoz-Chápuli, Coelomic epithelium-derived cells in visceral morphogenesis. *Dev. Dyn.* **245**, 307–322 (2016).
25. P. Dhakal, A. M. Kelleher, S. K. Behura, T. E. Spencer, Sexually dimorphic effects of forkhead box a2 (FOXA2) and uterine glands on decidualization and fetoplacental development. *Proc. Natl. Acad. Sci. U.S.A.* **117**, 23952–23959 (2020).
26. J. Goad, Y. A. Ko, M. Kumar, S. M. Syed, P. S. Tanwar, Differential Wnt signaling activity limits epithelial gland development to the anti-mesometrial side of the mouse uterus. *Dev. Biol.* **423**, 138–151 (2017).
27. A. Ferrer-Vaquer *et al.*, A sensitive and bright single-cell resolution live imaging reporter of Wnt/β-catenin signaling in the mouse. *BMC Dev. Biol.* **10**, 121 (2010).
28. Y. Sanchez-Ripoll *et al.*, Glycogen synthase kinase-3 inhibition enhances translation of pluripotency-associated transcription factors to contribute to maintenance of mouse embryonic stem cell self-renewal. *PLoS One* **8**, e60148 (2013).
29. M. Boretto *et al.*, Development of organoids from mouse and human endometrium showing endometrial epithelium physiology and long-term expandability. *Development* **144**, 1775–1786 (2017).
30. M. Kessler *et al.*, The Notch and Wnt pathways regulate stemness and differentiation in human fallopian tube organoids. *Nat. Commun.* **6**, 8989 (2015).
31. M. Y. Turco *et al.*, Long-term, hormone-responsive organoid cultures of human endometrium in a chemically defined medium. *Nat. Cell Biol.* **19**, 568–577 (2017).
32. A. Vlad-Fiegen, A. Langerak, S. Eberth, O. Müller, The Wnt pathway destabilizes adherens junctions and promotes cell migration via β-catenin and its target gene cyclin D1. *FEBS Open Bio* **2**, 26–31 (2012).
33. K. L. VanDussen *et al.*, Development of an enhanced human gastrointestinal epithelial culture system to facilitate patient-based assays. *Gut* **64**, 911–920 (2015).
34. R. P. Fordham *et al.*, Transplantation of expanded fetal intestinal progenitors contributes to colon regeneration after injury. *Cell Stem Cell* **13**, 734–744 (2013).
35. R. C. Mustata *et al.*, Identification of Lgr5-independent spheroid-generating progenitors of the mouse fetal intestinal epithelium. *Cell Rep.* **5**, 421–432 (2013).
36. L. Novellasdemunt *et al.*, NEDD4 and NEDD4L regulate Wnt signalling and intestinal stem cell priming by degrading LGR5 receptor. *EMBO J.* **39**, e102771 (2020).
37. Q. Yi *et al.*, Peroxiredoxin 4, a new oxidative stress marker in follicular fluid, may predict in vitro fertilization and embryo transfer outcomes. *Ann. Transl. Med.* **8**, 1049 (2020).
38. M. Uhlén *et al.*, Proteomics. Tissue-based map of the human proteome. *Science* **347**, 1260419 (2015).
39. Y. B. Chen, T. J. Cheng, H. H. Lin, Y. S. Yang, Spatial W-plasty full-thickness skin graft for neovaginal reconstruction. *Plast. Reconstr. Surg.* **94**, 727–731 (1994).
40. J. F. Kusiak, N. G. Rosenblum, Neovaginal reconstruction after exenteration using an omental flap and split-thickness skin graft. *Plast. Reconstr. Surg.* **97**, 775–781 (1996).
41. S. Haider *et al.*, Estrogen signaling drives ciliogenesis in human endometrial organoids. *Endocrinology* **160**, 2282–2297 (2019).
42. M. Zhu, T. Iwano, S. Takeda, Fallopian tube basal stem cells reproducing the epithelial sheets in vitro–Stem cell of fallopian epithelium. *Biomolecules* **10**, 1270 (2020).
43. S. C. Hewitt, K. S. Korach, Estrogen receptors: New directions in the new millennium. *Endocr. Rev.* **39**, 664–675 (2018).
44. A. M. Kelleher *et al.*, Forkhead box a2 (FOXA2) is essential for uterine function and fertility. *Proc. Natl. Acad. Sci. U.S.A.* **114**, E1018–E1026 (2017).
45. Y. You *et al.*, Role of f-box factor foxj1 in differentiation of ciliated airway epithelial cells. *Am. J. Physiol. Lung Cell. Mol. Physiol.* **286**, L650–L657 (2004).
46. H. Yoke *et al.*, Rsph4a is essential for the triplet radial spoke head assembly of the mouse motile cilia. *PLoS Genet.* **16**, e1008664 (2020).
47. V. H. Castleman *et al.*, Mutations in radial spoke head protein genes RSPH9 and RSPH4A cause primary ciliary dyskinesia with central-microtubular-pair abnormalities. *Am. J. Hum. Genet.* **84**, 197–209 (2009).
48. A. C. Merveille *et al.*, CCDC39 is required for assembly of inner dynein arms and the dynein regulatory complex and for normal ciliary motility in humans and dogs. *Nat. Genet.* **43**, 72–78 (2011).
49. M. Karlsson *et al.*, A single-cell type transcriptomics map of human tissues. *Sci. Adv.* **7**, eabh2169 (2021).
50. M. Kumar, S. M. Syed, M. M. Taketo, P. S. Tanwar, Epithelial Wnt/βcatenin signalling is essential for epididymal coiling. *Dev. Biol.* **412**, 234–249 (2016).
51. S. M. Syed *et al.*, Endometrial Axin2+ cells drive epithelial homeostasis, regeneration, and cancer following oncogenic transformation. *Cell Stem Cell* **26**, 64–80.e13 (2020).
52. G. D. Orvis, R. R. Behringer, Cellular mechanisms of Müllerian duct formation in the mouse. *Dev. Biol.* **306**, 493–504 (2007).
53. D. K. Boruah *et al.*, Spectrum of MRI appearance of Mayer-Rokitansky-Kuster-Hauser (MRKH) syndrome in primary amenorrhea patients. *J. Clin. Diagn. Res.* **11**, TC30–TC35 (2017).
54. G. R. Cunha *et al.*, Development of the human female reproductive tract. *Differentiation* **103**, 46–65 (2018).
55. K. Lõhmussaar *et al.*, Patient-derived organoids model cervical tissue dynamics and viral oncogenesis in cervical cancer. *Cell Stem Cell* **28**, 1380–1396.e6 (2021).
56. A. Ali *et al.*, Cell lineage tracing identifies hormone-regulated and Wnt-responsive vaginal epithelial stem cells. *Cell Rep.* **30**, 1463–1477.e7 (2020).
57. Committee on Adolescent Health Care, ACOG Committee Opinion No. 728: Müllerian agenesis: Diagnosis, management, and treatment. *Obstet. Gynecol.* **131**, e35–e42 (2018).
58. M. Nisolle, J. Donnez, Vaginoplasty using amniotic membranes in cases of vaginal agenesis or after vaginectomy. *J. Gynecol. Surg.* **8**, 25–30 (1992).
59. S. F. Badylak, D. O. Freytes, T. W. Gilbert, Reprint of: Extracellular matrix as a biological scaffold material: Structure and function. *Acta Biomater.* **23**, S17–S26 (2015).
60. S. Noguchi *et al.*, Use of artificial dermis and recombinant basic fibroblast growth factor for creating a neovagina in a patient with Mayer-Rokitansky-Kuster-Hauser syndrome. *Hum. Reprod.* **19**, 1629–1632 (2004).
61. A. Kobayashi, R. R. Behringer, Developmental genetics of the female reproductive tract in mammals. *Nat. Rev. Genet.* **4**, 969–980 (2003).
62. G. R. Cunha, Mesenchymal-epithelial interactions: Past, present, and future. *Differentiation* **76**, 578–586 (2008).
63. W. Winuthayanon, S. C. Hewitt, G. D. Orvis, R. R. Behringer, K. S. Korach, Uterine epithelial estrogen receptor α is dispensable for proliferation but essential for complete biological and biochemical responses. *Proc. Natl. Acad. Sci. U.S.A.* **107**, 19272–19277 (2010).
64. T. Kurita, P. S. Cooke, G. R. Cunha, Epithelial-stromal tissue interaction in paramesonephric (Müllerian) epithelial differentiation. *Dev. Biol.* **240**, 194–211 (2001).
65. C. Miller, D. A. Sassoon, Wnt-7a maintains appropriate uterine patterning during the development of the mouse female reproductive tract. *Development* **125**, 3201–3211 (1998).
66. J. A. Hernandez Gifford, M. E. Hunzicker-Dunn, J. H. Nilson, Conditional deletion of beta-catenin mediated by Amhr2cre in mice causes female infertility. *Biol. Reprod.* **80**, 1282–1292 (2009).
67. T. Wiwatpanit *et al.*, Scaffold-free endometrial organoids respond to excess androgens associated with polycystic ovarian syndrome. *J. Clin. Endocrinol. Metab.* **105**, 769–780 (2020).
68. M. Hofer, M. P. Lutolf, Engineering organoids. *Nat. Rev. Mater.* **6**, 402–420 (2021).
69. L. Cordero-Espinoza *et al.*, Dynamic cell contacts between periportal mesenchyme and ductal epithelium act as a rheostat for liver cell proliferation. *Cell Stem Cell* **28**, 1907–1921.e8 (2021).
70. R. Lim *et al.*, Preliminary characterization of voltage-activated whole-cell currents in developing human vestibular hair cells and calyx afferent terminals. *J. Assoc. Res. Otolaryngol.* **15**, 755–766 (2014).
71. V. D. Venkata *et al.*, Data for "Development and characterization of human fetal female reproductive tract organoids to understand Müllerian duct anomalies." Accession # MSV000088200. MassIVE. https://massive.ucsd.edu/ProteoSAFe/dataset.jsp?task=cfa2d8d92b07421ab166878ccb8e192f. Accessed 11 July 2022.